Characteristics and instabilities of mode-locked quantum-dot diode lasers

Yan Li,[2] Luke. F. Lester,[2] Derek Chang,[3] Carsten Langrock,[3] M. M. Fejer[3] and Daniel J. Kane[1,*]

[1]*Mesa Photonics LLC., 1550 Pacheco St., Santa Fe, NM 87505,USA*
[2]*Center for High Technology Materials, The University of New Mexico, 1313 Goddard SE, Albuquerque, NM 87106, USA*
[3]*E. L. Ginzton Laboratory, Stanford University, Stanford, California CA 94305, USA*
[*]*djkane@mesaphotonics.com*

Abstract: Current pulse measurement methods have proven inadequate to fully understand the characteristics of passively mode-locked quantum-dot diode lasers. These devices are very difficult to characterize because of their low peak powers, high bandwidth, large time-bandwidth product, and large timing jitter. In this paper, we discuss the origin for the inadequacies of current pulse measurement techniques while presenting new ways of examining frequency-resolved optical gating (FROG) data to provide insight into the operation of these devices. Under the assumptions of a partial coherence model for the pulsed laser, it is shown that simultaneous time-frequency characterization is a necessary and sufficient condition for characterization of mode-locking. Full pulse characterization of quantum dot passively mode-locked lasers (QD MLLs) was done using FROG in a collinear configuration using an aperiodically poled lithium niobate waveguide-based FROG pulse measurement system.

OCIS codes: (140.4050) Mode-locked lasers; (140.5960) Semiconductor lasers; (130.3120) Integrated optics devices.

References and Links

1. E. U. Rafailov, M. A. Cataluna, and W. Sibbett, "Mode-locked quantum-dot lasers," Nat. Photonics **1**(7), 395–401 (2007).
2. D. Bimberg, N. Kirstaedter, N. N. Ledentsov, Zh. I. Alferov, P. S. Kop'ev, and V. M. Ustinov, "InGaAs-GaAs quantum-dot Lasers," IEEE J. Sel. Top. Quantum Electron. **3**(2), 196–205 (1997).
3. X. D. Huang, A. Stintz, H. Li, L. F. Lester, J. Cheng, and K. J. Malloy, "Passive mode-locking in 1.3-μm two-section InAs quantum dot lasers," Appl. Phys. Lett. **78**(19), 2825–2827 (2001).
4. Y.-C. Xin, Y. Li, V. Kovanis, A. L. Gray, L. Zhang, and L. F. Lester, "Reconfigurable quantum dot monolithic multisection passive mode-locked lasers," Opt. Express **15**(12), 7623–7633 (2007).
5. C.-Y. Lin, Y.-C. Xin, Y. Li, F. L. Chiragh, and L. F. Lester, "Cavity design and characteristics of monolithic long-wavelength InAs/InP quantum dash passively mode-locked lasers," Opt. Express **17**(22), 19739–19748 (2009).
6. D. B. Malins, A. Gomez-Iglesias, S. J. White, W. Sibbett, A. Miller, and E. U. Rafailov, "Ultrafast electroabsorption dynamics in an InAs quantum dot saturable absorber at 1.3 μm," Appl. Phys. Lett. **89**(17), 171111 (2006).
7. M. G. Thompson, A. R. Rae, Mo Xia, R. V. Penty, and I. H. White, "InGaAs quantum-dot mode-locked laser diodes," IEEE J. Sel. Top. Quantum Electron. **15**(3), 661–672 (2009).
8. D. Bimberg, M. Grundmann, N. N. Ledentsov, S. S. Ruvimov, P. Werner, U. Richter, J. Heydenreich, V. M. Ustinov, P. S. Kop'ev, and Z. I. Alferov, "Self-organization processes in MBE-grown quantum dot structures," Thin Solid Films **267**(1-2), 32–36 (1995).
9. D. Bimberg, "Quantum dot based nanophotonics and nanoelectronics," Electron. Lett. **44**(3), 168–171 (2008).
10. L. Zhang, L.-S. Cheng, A. L. Gray, H. Huang, S. Kutty, H. Li, J. Nagyvary, F. Nabulsi, L. Olona, E. Pease, Q. Sun, C. Wiggins, J. C. Zilko, Z. Zou, and P. M. Varangis, "High-power low-jitter quantum-dot passively modelocked lasers," Proc. SPIE **6115**, 611502, 611502-8 (2006).
11. G. A. Keeler, B. E. Nelson, D. Agarwal, C. Debaes, N. C. Helman, A. Bhatnagar, and D. A. B. Miller, "The benefits of ultrashort optical pulses in optically interconnected systems," IEEE J. Sel. Top. Quantum Electron. **9**(2), 477–485 (2003).
12. A. A. Aboketaf, A. W. Elshaari, and S. F. Preble, "Optical time division multiplexer on silicon chip," Opt. Express **18**(13), 13529–13535 (2010).

#177027 - $15.00 USD Received 28 Sep 2012; revised 24 Nov 2012; accepted 12 Mar 2013; published 26 Mar 2013

13. M. Mielke, G. A. Alphonse, and P. J. Delfyett, "168 channels x 6 GHz from a multiwavelength mode-locked semiconductor laser," IEEE Photon. Technol. Lett. **15**(4), 501–503 (2003).
14. Y. Li, F. L. Chiragh, Y.-C. Xin, C.-Y. Lin, J. Kim, C. G. Christodoulou, and L. F. Lester, "Harmonic mode-locking using the double interval technique in quantum dot lasers," Opt. Express **15**, 7623–7633 (2010).
15. C.-Y. Lin, Y.-C. Xin, J. H. Kim, C. G. Christodoulou, and L. F. Lester, "Compact optical generation of microwave signals using a monolithic quantum dot passively mode-locked laser," IEEE Photon. Journal **1**(4), 236–244 (2009).
16. M. Xia, M. G. Thompson, R. V. Penty, and I. H. White, "External-cavity mode-locked quantum-dot lasers for low repetition rate, sub-picosecond pulse generation," presented at the Lasers Elect.-Opt. (CLEO) Conf. San Jose, CA, 2008.
17. C.-Y. Lin, F. Grillot, Y. Li, R. Raghunathan, and L. F. Lester, "Characterization of timing jitter in a 5 GHz quantum dot passively mode-locked laser," Opt. Express **18**(21), 21932–21937 (2010).
18. M. G. Thompson, R. V. Penty, and I. H. White, "Regimes of modelocking in tapered quantum dot laser diodes," in Proc. Semicond. Laser Conf. (ISLC), Sorrento, Italy, Sep. 2008, pp. 27–28.
19. Y.-C. Xin, D. J. Kane, and L. F. Lester, "Frequency-resolved optical gating characterisation of passively modelocked quantum-dot laser," Electron. Lett. **44**(21), 1255–1256 (2008).
20. H. Schmeckebier, G. Fiol, C. Meuer, D. Arsenijević, and D. Bimberg, "Complete pulse characterization of quantum dot mode-locked lasers suitable for optical communication up to 160 Gbit/s," Opt. Express **18**(4), 3415–3425 (2010).
21. G. Fiol, C. Meuer, H. Schmeckebier, D. Arsenijevic, S. Liebich, M. Laemmlin, M. Kuntz, and D. Bimberg, "Quantum-dot semiconductor mode-locked lasers and amplifiers at 40 GHz," IEEE J. Quantum Electron. **45**(11), 1429–1435 (2009).
22. N. Rebrova, T. Habruseva, G. Huyet, and S. P. Hegarty, "Stabilization of a passively mode-locked laser by continuous wave optical injection," Appl. Phys. Lett. **97**(10), 101105 (2010).
23. T. Habruseva, S. O'Donoghue, N. Rebrova, D. A. Reid, L. P. Barry, D. Rachinskii, G. Huyet, and S. P. Hegarty, "Quantum-dot mode-locked lasers with dual-mode optical injection," IEEE Photon. Technol. Lett. **22**(6), 359–361 (2010).
24. J. Ratner, G. Steinmeyer, T. C. Wong, R. Bartels, and R. Trebino, "Coherent artifact in modern pulse measurements," Opt. Lett. **37**(14), 2874–2876 (2012).
25. D. J. Kane and R. Trebino, "Characterization of arbitrary femtosecond pulses using frequency -resolved optical gating," IEEE J. Quantum Electron. **29**(2), 571–579 (1993).
26. R. Trebino, K. W. DeLong, D. N. Fittinghoff, J. N. Sweetser, M. A. Krumbugel, B. A. Richman, and D. J. Kane, "Measuring ultrashort laser pulses in the time-frequency domain using frequency-resolved optical gating," Rev. Sci. Instrum. **68**(9), 3277–3295 (1997).
27. B. Kohler, V. V. Yakovlev, K. R. Wilson, J. Squier, K. W. Delong, and R. Trebino, "Phase and intensity characterization of femtosecond pulses from a chirped-pulse amplifier by frequency-resolved optical gating," Opt. Lett. **20**(5), 483–485 (1995).
28. M. Photonics, "FROG scan screen captures of shaped pulses," *http://www.mesaphotonics.com/products-2/pulse-measurement/frogscan-data/*.
29. R. Trebino, *Frequency-Resolved Optical Gating: The Measurement of Ultrashort Laser Pulses* (Kluwer Academic, 2000).
30. T. Pfeifer, Y. Jiang, S. Düsterer, R. Moshammer, and J. Ullrich, "Partial-coherence method to model experimental free-electron laser pulse statistics," Opt. Lett. **35**(20), 3441–3443 (2010).
31. S.-D. Yang, A. M. Weiner, K. R. Parameswaran, and M. M. Fejer, "Ultrasensitive second-harmonic generation frequency-resolved optical gating by aperiodically poled $LiNbO_3$ waveguides at 1.5 microm," Opt. Lett. **30**(16), 2164–2166 (2005).
32. I. Amat-Roldán, I. G. Cormack, P. Loza-Alvarez, E. Gualda, and D. Artigas, "Ultrashort pulse characterisation with SHG collinear-FROG," Opt. Express **12**(6), 1169–1178 (2004).

1. Introduction

Mode-locking has been observed in a variety of diode laser structures. Compared to bulk or quantum well materials, self-assembled quantum dot (QD) materials provide several advantages [1–5]: ultrafast carrier dynamics and low saturation energy for wide range mode-locking [6,7], an inhomogeneously broadened gain spectrum for narrow pulse duration [8,9]; and discrete energy levels and a low transparency current for low timing jitter [10]. These traits make monolithic quantum dot passively mode-locked lasers (QD MLLs) promising candidates for applications such as inter-chip/intra-chip clock distribution [11], high bit-rate optical time division multiplexing [12,13], and diverse waveform generation [14,15]. In 2001, Huang *et. al* demonstrated [3], for the first time, a monolithic two-section QD MLL that had a repetition rate of 7.4 GHz with a pulse duration of 17 ps. Since then, monolithic QD MLLs have been investigated for over a decade, and all the characteristics of QD MLLs have steadily improved. The reported repetition rates range from 300 MHz to 240 GHz [7, 16], and the pulse timing jitter is down to 96 fs [17]. A sub-ps pulse duration of 391 fs from a QD

#177027 - $15.00 USD Received 28 Sep 2012; revised 24 Nov 2012; accepted 12 Mar 2013; published 26 Mar 2013

MLL was reported for the first time by Rafailov et. al in 2005 [1]. After that, Thompson et. al demonstrated a pulse width as short as 360 fs using a tapered waveguide section [18]. In both cases, the pulse durations were measured using the second harmonic generation (SHG) intensity autocorrelation method. Ultrashort pulses from QD MLLs with similar material systems and device configurations have been characterized by other groups using more complete pulse characterization tools such as frequency resolved optical gating (FROG). However, pulse widths reported by these groups are only in the range of a few picoseconds [19–23]. While QD mode-locked lasers are used in this work, the conclusions regarding pulse measurement and mode-locking criteria should be applicable to all mode-locked lasers.

Passively mode-locked semiconductor diode lasers present unique challenges for pulse measurement. Saturation intensities of the semiconductor gain media are much lower than other solid-state materials. Cavity output coupling is high, reducing the photon lifetime to less than a single round trip. As a result, timing jitter is a significant percentage of the pulse duration. This coupled with the fact that peak powers are on the order of 1 W, typically force pulse measurement diagnostics to be indirect.

One method of choice among the mode-locked diode laser community is autocorrelation, which is immune to timing jitter, but often leads to erroneous results. Sampling oscilloscopes are nearly fast enough for pulse measurement, but they provide only an average pulse envelope. FROG-based measurements have been made, but only for close to ideal situations [19]. Frequency-Resolved Mach-Zehnder Gating (FRMZG) measurements require injection locked lasers to lower the timing jitter enough for measurements to be successful while FROG measurements have only been successful for specific devices [19–23].

The reason for the lack of measurement success has not been clear. Sampling oscilloscopes and autocorrelations show smooth profiles. FROG traces are often smooth and simple, but the algorithm often fails to converge [24]. While the blame is often placed on the FROG technique, FROG has been shown to converge well for much more complex pulses than measured FROG traces from passively mode-locked diode lasers would indicate [25–28]. Indeed, FROG measurements of highly stable, low jitter lasers have not been shown to be problematic [29].

In this work, we develop a highly sensitive FROG ultrafast pulse measurement system specifically designed for measuring pulses from mode-locked quantum dot diode lasers. From the measurements obtained, we conclude that the cause for the discrepancies in measurement methods lies in the unstable nature of the passively mode-locked diode lasers themselves—pulse characteristics are surprisingly similar to models proposed to explain pulse-pulse fluctuations in free electron X-ray lasers [30]. Because all pulse measurement techniques require some assumptions to make correct measurements, we assert that instabilities in mode-locked diode lasers violate assumptions required for every pulse measurement method to be rigorously valid. In spite of this, if pulse measurement tools are used knowing that assumptions are violated, much can be learned about these devices. For example, our FROG measurements of the mode-locked diode lasers show below that pulse-to-pulse structure can be highly variable even when pulse-to-pulse jitter is low.

2. Device description and experimental setup

The InAs/InGaAs QD MLLs that were studied in this work were grown on a GaAs substrate using Molecular Beam Epitaxy (MBE) [4]. The “Dots-in-a-well (DWELL)” active region consists of 8 stacks of self-assembled InAs quantum dots embedded in InGaAs quantum wells. A 4-μm wide ridge waveguide two-section laser was fabricated following standard edge-emitting laser processing steps. The electrical isolation between sections was realized by proton implantation. The total cavity length is 8.3 mm, and the absorber is 1.0-mm long. This cavity length gives a fundamental repetition rate of 5 GHz. The device’s back facet, which is near the absorber, has an HR-coating with a reflectivity of approximately 95%. The other facet is low reflection (LR)-coated with a reflectivity of about 5%. The two-section laser was mounted on an AlN substrate and then onto a copper heatsink that was thermo-electrically cooled to 20 °C. For cases where the absorber was reverse biased from 4 to 5 V, the threshold

#177027 - $15.00 USD Received 28 Sep 2012; revised 24 Nov 2012; accepted 12 Mar 2013; published 26 Mar 2013

current was 90 mA and the slope efficiency was 0.27 W/A. The emission wavelength is about 1242 nm.

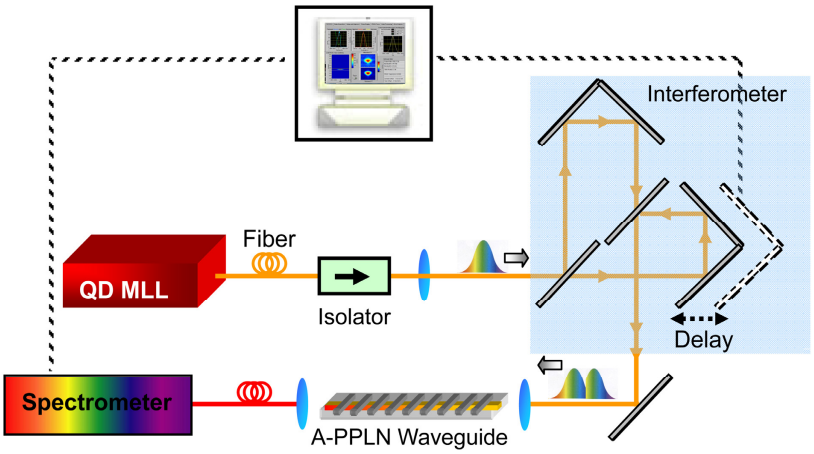

Fig. 1. Schematic diagram of the collinear SHG FROG system.

The schematic diagram of the collinear SHG FROG system is shown in Fig. 1. It is based on previous work by Yang *et al.* [31]. The optical output of the laser was collected with an optical head, which integrates a lens, an isolator and a short 1-m single-mode polarization-maintaining (PM) fiber pigtail that is then coupled into the FROG system. At the input of the FROG system, a fiber collimator couples the pulse train into a free-space Michelson interferometer (MI) to produce pulse pairs with variable delay that are coupled into an a-periodically-poled $LiNO_3$ (A-PPLN) waveguide with a 45.4 mm long poling region to produce a SHG signal. 40X microscope objectives were used for coupling light into and out of the waveguide. The position of the servo is under closed loop control using an optical position sensitive detector, which provides a delay resolution of 3.5 fs.

The A-PPLN chip improves SHG conversion efficiency of the mode-locked diode lasers to a level that allows near real-time data acquisition. A single A-PPLN chip contained several uniform and chirped poled gratings. With apodization, the bandwidth of the chirped poled grating waveguides was nearly flat over 20 nm. The total waveguide length including mode-filters and tapers into the QPM region was 52 mm long. Four different wavelength regions were available on each chip providing wavelength coverage from 1215 nm – 1280 nm. Center wavelengths of the waveguides were 1225 nm, 1240 nm, 1255 nm, and 1270 nm. Because widely tunable, high power sources were not available the exact waveguide SHG efficiency was not measured. However, by comparing the original QD MLL wavelength spectrum with the value computed from the FROG measurement, the bandwidth of the A-PPLN is verified to be sufficiently wide. In addition, no spectral artifacts from the A-PPLN pass band were observed and measured FROG traces using the waveguides were very close to FROG traces measured previously [19] using the same mode-locked laser. The A-PPLN based system is much more sensitive, and we estimate its sensitivity to be better than 3×10^{-5} W^2 (peak power multiplied by average power) for a 20 second acquisition. The system discussed in [19] required a 30-45 minute acquisition to achieve the same sensitivity.

Because the servo is under closed loop control, the servo maintains fixed delays indefinitely and can be step scanned. At each relative time delay between the two pulse replicas, an SHG spectrum is recorded using an Ocean Optics QE65000 spectrometer. Integration time could be adjusted to optimize signal levels. The FROG trace is constructed from 64, 128, or 256 different equally spaced relative time delays ("grid size") and resampled in the wavelength axis to a constant frequency spacing of $1/(N\Delta t)$ where N is the grid size and Δt is the relative time spacing.

#177027 - $15.00 USD Received 28 Sep 2012; revised 24 Nov 2012; accepted 12 Mar 2013; published 26 Mar 2013

Because of the collinear geometry, interference fringes are produced. The servo position is determined by the sum of the voltage on an internal DAC and an external analog input voltage. By applying an AC modulation to the servo position using the external analog input, the delay is modulated, and the fringes are averaged out by using the integration time of the spectrometer as a low pass filter. The DC background from the low pass filtered FROG trace is removed using background subtraction [31,32]. The data acquisition, preprocessing and processing was done using commercial FROG software that was developed by Mesa Photonics.

3. Pulse measurement of QDMLLs

In Fig. 2(a), the SHG FROG trace from the QD laser is shown when the gain section is biased at 105 mA and the absorber is biased at –4.5 V. (SHG FROG traces are symmetric about t = 0.) The FROG trace constructed from the pulse retrieved from this FROG trace is shown in Fig. 2(b). An excellent agreement between both traces is observed. The FROG trace error is 0.95%,

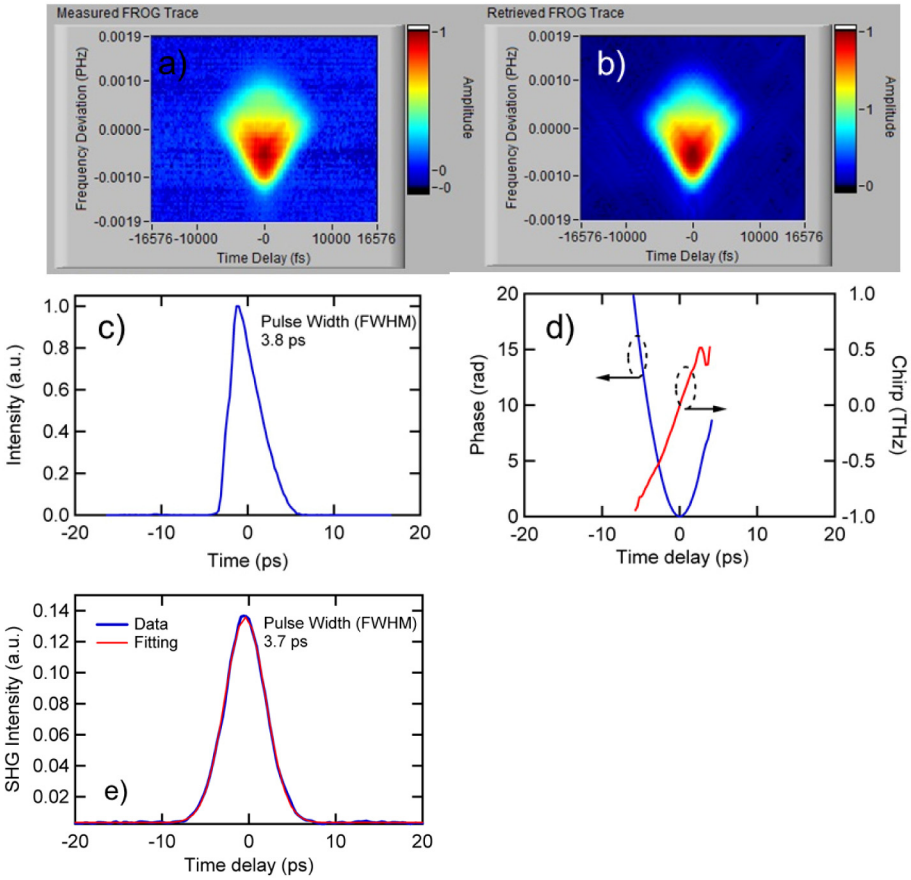

Fig. 2. (a) Measured and (b) retrieved FROG spectrograms of the passive-mode-locked laser at 105 mA gain section current and –4.5 V absorber section reverse bias. (c) Retrieved pulse intensity profile. (d) phase profile and temporal chirp; (e) Pulse trace measured by autocorrelator at the same bias condition.

which is defined by the average RMS per pixel error. The time-domain pulse intensity and phase profile derived from the FROG traces are shown in Figs. 2(c) and 2(d), respectively. The FWHM of the time domain intensity is 3.8 ps. The pulse has an asymmetric shape with a

#177027 - $15.00 USD Received 28 Sep 2012; revised 24 Nov 2012; accepted 12 Mar 2013; published 26 Mar 2013

fast leading edge and a slow trailing one and agrees with previous FROG measurements on this QDMLL [19]. The reason for the steeply rising edge is due to stronger absorption in the saturable absorber, and the broadened pulse in the gain section forms the slow tail. The instantaneous frequency is the derivative of the temporal phase and is plotted in Fig. 2(d). It shows that the pulses from the QDMLL are predominantly linearly-chirped. As a comparison, the pulse shapes obtained from the autocorrelator are shown in Fig. 2(e) when the QD MLL was biased at the same conditions as above. The autocorrelation trace is symmetric and has a deconvoluted FWHM of 3.7 ps if the original pulse is assumed to be Gaussian (and symmetric).

As a limiting case, FROG traces obtained using higher drive currents contained coherence spikes. Figure 3(a) shows measured FROG raw trace when the gain current is 135 mA and the reverse bias is –4.5 V. The narrow darker region at the center of FROG trace indicates a strong coherence spike at zero time delay. The phase retrieval algorithm of the FROG failed to converge under this condition, and a temporal pulse profile could not be obtained. However, mode-locked behavior is still indicated by autocorrelation, which is shown in Fig. 3(b). A coherence spike is visible on the autocorrelation, and the autocorrelation cannot be described by a Gaussian function. Coherence spikes are well known in autocorrelation traces and are believed to be caused by laser instabilities. This idea is corroborated by the inability of the phase retrieval algorithm to converge for FROG traces containing coherence spikes. The latter occurs because even random noise is always coherent at zero time delay, causing a large spike to occur at zero time delay where pulse replicas overlap. In the case of true noise, the correlation function goes to zero at non-zero time delays. Non-random noise has lower correlation values at a non-zero time delay. If the pulse breakup is stable, then patterning of the FROG trace and stable structure in the FROG measurement appear (see Fig. 5 in Section 4). Patterning was not observed in any FROG trace measured, indicating instability in individual pulse structure. This implies that FROG has a stricter condition for defining stable mode-locking than the autocorrelation method.

Figure 4 is a comparison between the mode-locking operation map obtained using FROG measurements and using auotocorrelation that illustrates FROG's more strict condition for stable mode-locking and the effect pulse measurement choices have on conclusions regarding

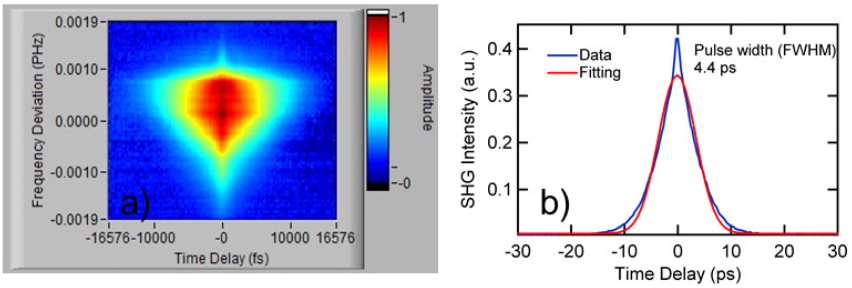

Fig. 3. (a) Measured FROG spectrogram of the passive-mode-locked laser at 135 mA gain section current and –4.5 V absorber section reverse bias. (b) Pulse trace measured by autocorrelation.

laser performance. Figure 4(a) shows the stable mode-locking operation map where the FROG trace error is smaller than 2% (greater than 2% error was deemed "not converged" or a sufficiently low quality measurement for purposes of this comparison) and the pulse width is smaller than 10 ps as measured using FROG. The pulse width is represented by a color bar. The smallest pulse width as measured by FROG is 2.7 ps at the condition of 95 mA gain current and –4.5 V reverse bias. The two blue circles marked as "A" and "B" correspond to the two different bias conditions in Fig. 2 and Fig. 3, respectively. As a comparison, an operational map where the pulse width is smaller than 10 ps as determined by autocorrelation is plotted in Fig. 4(b). It should be stated here that because the pulse shape is unknown in

#177027 - $15.00 USD Received 28 Sep 2012; revised 24 Nov 2012; accepted 12 Mar 2013; published 26 Mar 2013

autocorrelation, criteria for determining mode-locked regions in conventional operational maps are largely arbitrary and the mode-locked region given by autocorrelation can be set much wider than that determined by FROG; most of the bias conditions outside the FROG converged region actually correspond to unstable mode-locking behavior. Autocorrelation's misleading conclusions are discussed in more detail in the next section.

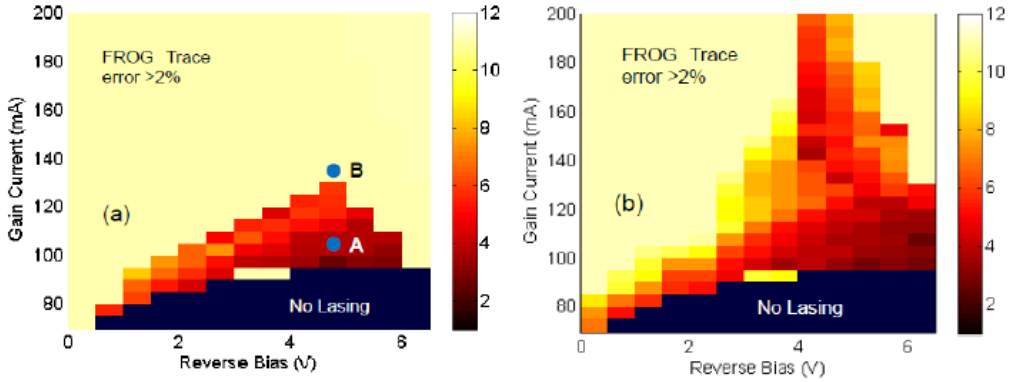

Fig. 4. Pulse FWHM of the QD MLL as a function of gain current and reverse bias measured by (a) the FROG and the retrieval error of the algorithm is smaller than 2%. (b) Autocorrelation results showing the regions predicted to have less than 10 ps pulse width. The two blue circles marked as "A" and "B" in Fig. 4(a) corresponds to the two different bias conditions in Fig. 2 and Fig. 3, respectively. The smallest pulse width is 2.7 ps as measured by FROG when the gain current is 95 mA and reverse bias is –4.5 V.

4. FROG traces of noisy pulse trains

When measuring pulses using virtually all pulse measurement techniques, from digital sampling oscilloscopes to FROG, stability of the pulse train is implied; each pulse is identical to the previous pulse and the next pulse. Depending on the technique, failure to have identical pulses can result in erroneous results, incorrect conclusions, or failure of the method to make a measurement. In the case of FROG, instability of the pulse train results in the failure to make a measurement—the algorithm fails to converge. In the case of a digital sampling oscilloscope, for example, the sampled average of the pulse train is recorded. If assumed to be the actual pulse train, resulting conclusions may be incorrect. In the case of autocorrelation, the average autocorrelation is recorded, which again, may lead to incorrect conclusions. Consequently, using multiple pulse measurement techniques will result in inconsistent measurements. In this section, we show how FROG can be used to explain inconsistencies when using multiple pulse measurement schemes.

Because FROG measures pulses using a simultaneous time-frequency methodology, even slight variations in the pulse characteristics result in different spectrograms. Indeed, FROG spectrograms are unique signatures of the pulses they represent [29]. FROG Spectrograms add linearly in intensity, not in pulse characteristics; while average spectrograms can be formed, a pulse corresponding to the averaged spectrogram rarely exists especially when the partial coherence model applies because pulse structure is highly variable. Shown in Fig. 5 are pulse examples and corresponding spectrograms illustrating this premise.

Figure 5(a) shows two plots. The red line is a sample of a pulse formed from random noise modulated by a Gaussian. Summing 10,000 of such pulses results in the Gaussian modulation function (black line). An average autocorrelation of the noisy pulse train is shown in Fig. 5(b). A coherence spike is clearly visible. While coherence spikes are indicative of high frequency structure in a pulse, they are not necessarily indicative of fluctuating structure;

#177027 - $15.00 USD Received 28 Sep 2012; revised 24 Nov 2012; accepted 12 Mar 2013; published 26 Mar 2013

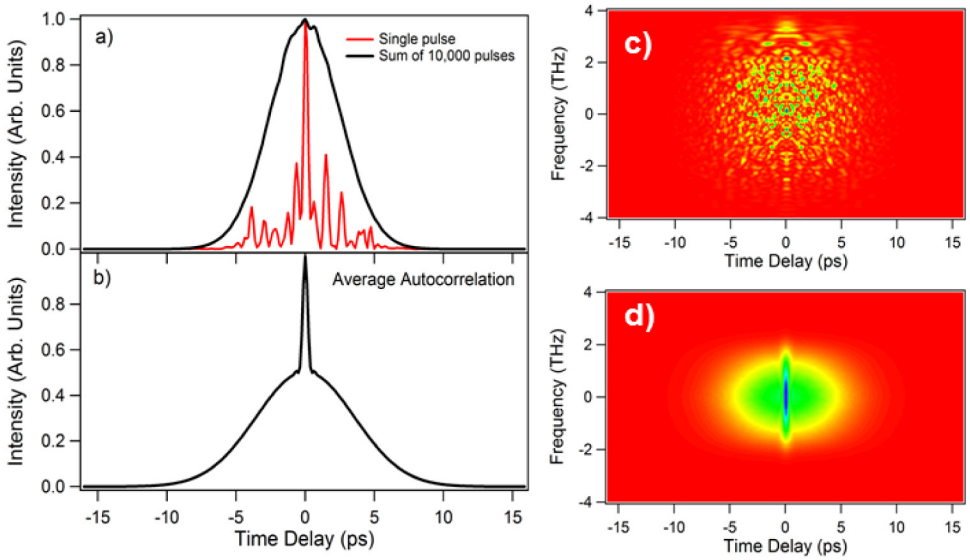

Fig. 5. Example noisy pulses and FROG traces. a) shows the sum of 10,000 noisy pulses (black) and a sample single noisy pulse (red) formed from random noise modulated by a Gaussian. b) shows the average autocorrelation of a noisy pulse train. c) shows the FROG trace of a pulse train comprising of only pulses depicted by the red line in a). d) shows the average FROG trace of a noisy pulse train. While the single pulse shown in part a) can be extracted from the FROG trace shown in c), no pulse can be extracted from the FROG trace in part d).

similar looking autocorrelations can be formed from a stable, noisy pulse train, where each noisy pulse is identical [29]. Thus, a smooth autocorrelation may result from an either a stable pulse train or an unstable one resulting in an inconclusive measurement. Only a simultaneous time-frequency measurement can differentiate between stable and unstable conditions when the partial coherence model applies. Because of uniqueness, even slight differences in peak levels will generate a different spectrogram. Indeed, when the partial coherence model applies, a smooth FROG spectrogram can be constructed only from the sum of many vastly different FROG spectrograms representing vastly different pulses.

Figure 5(c) (upper right) shows a FROG trace of a stable pulse train of identical, highly structured noise pulses formed from the pulse shown in Fig. 5(a) (red line). While the FROG trace itself is highly structured, it is stable, and the retrieval algorithm will converge to the pulse shown in Fig. 5(a). A coherence spike is not visible unless the FROG trace is integrated along the frequency axis to form the autocorrelation (Fig. 5(b)).

Figure 5(d) shows how the FROG trace of an average of 10,000 different noisy pulses would appear. Unlike the FROG trace of the single noisy pulse, the coherence spike becomes visible and the FROG trace is very smooth. However, this FROG trace corresponds to no single pulse. It can be formed only from an incoherent average of an ensemble of different noisy pulses. Without surprise, the retrieval algorithm fails to converge and cannot extract a pulse from it.

5. Partial coherence noise pulse model

While failing to extract a pulse from a FROG trace is not a weakness, it does require additional constraints to extract system information from the FROG trace. In the case of the mode-locked quantum dot diode lasers, we can conclude that the mode-locking behavior of the laser while obtaining the FROG trace shown in Fig. 2(a) is stable and the pulse train consists of pulses with characteristics shown in Figs. 2(c) and 2(d). When the retrieval algorithm fails to converge, as in the case of Fig. 3(a), we conclude that because the FROG trace is smooth, the coherence spike is plainly visible and the FROG algorithm fails to

#177027 - $15.00 USD Received 28 Sep 2012; revised 24 Nov 2012; accepted 12 Mar 2013; published 26 Mar 2013

converge, the laser is not stably mode-locked. This conclusion is important, but more information is desirable; good pulse measurement technology should provide more.

Even though the FROG algorithm fails to extract a pulse from the FROG trace shown in Fig. 3(a), it only does so because the assumptions of a stable pulse train are not satisfied. On the other hand, if we assume a model for the laser output, we can bypass the algorithm completely and glean additional information from the FROG traces. Admittedly, this information is more qualitative than quantitative, but useful nonetheless.

To extract information directly from the FROG traces without using the algorithm, we need to have a semi-empirical model to explain measured FROG traces. We adapt a previously published partial coherence model explaining observations in free-electron lasers where pulses grow from noise to explain the observed FROG measurements of quantum dot diode lasers [30]. To apply this model to QDMLLs, we first assume a spectral phase and a spectral shape determined by the gain profile of the gain medium (in this work we use a Gaussian gain profile). We start with random noise and apply a duration limit. The next step is to apply the spectral constraint of the gain profile and the spectral phase. The last step is to apply the saturable absorber constraint in the time domain by extinguishing the leading edge of the pulse until a specific integrated intensity is achieved.

Shown in Fig. 6 are FROG traces obtained from applying different spectral phases. Figure 6(a) shows a FROG trace with flat spectral phase; Fig. 6(b) is a FROG trace with only cubic spectral phase. Whereas the FROG traces with no chirp (Fig. 6(a)) and only cubic chirp (Fig. 6(b)) appear very different from the measured FROG traces shown in Figs. 2 and 3, when linear chirp is added, the FROG trace takes a shape very similar to the FROG trace shown in Fig. 3(a) with a coherence spike that is clearly visible. Adding cubic spectral phase shapes the FROG trace slightly (Fig. 6(d)) making it qualitatively more like Fig. 3(a), but failing to match the shape on the bottom. Thus, other factors, unaccounted for in this simple model, are shaping the FROG trace. In spite of these details, the match is surprising close for a simple model.

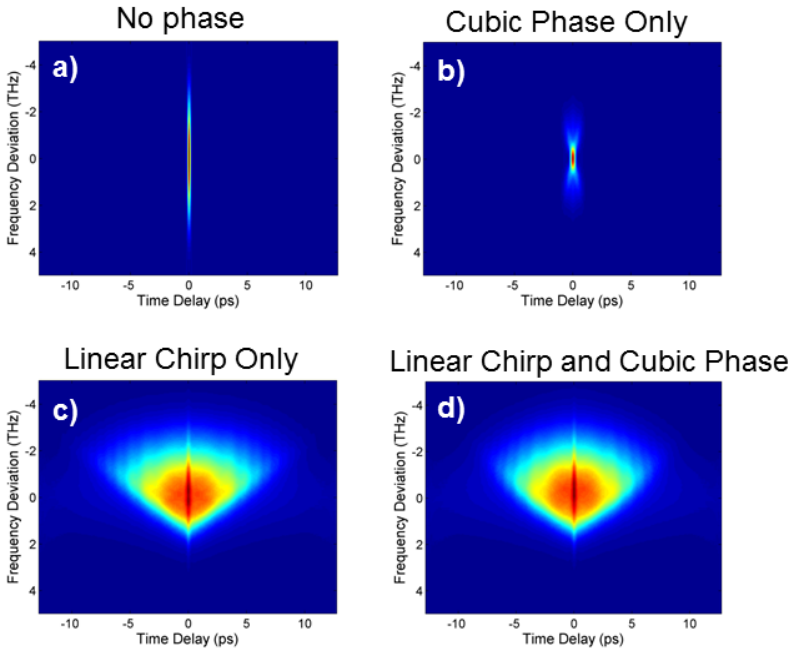

Fig. 6. FROG traces constructed from the partial coherence model described in the text. a) no spectral phase; b) cubic spectral phase only. c) has linear chirp only, and d) has linear and cubic chirp. All of the examples use the same spectral gain profile.

#177027 - $15.00 USD Received 28 Sep 2012; revised 24 Nov 2012; accepted 12 Mar 2013; published 26 Mar 2013

Because pulses are formed in the model, average temporal shapes and spectral shapes as shown Fig. 7 can be determined. These are the ones that would be measured by a sampling oscilloscope (temporal) or an optical spectrum analyzer (spectral). Figure 7(a) shows the pulse with flat spectral phase. It is quite short, the transform limit of the average pulse spectrum (Fig. 7(d)), which is roughly the laser gain profile used. Adding spectral phase to the model begins to shape the average pulse spectrum (Fig. 7(e)) as shown by the addition of cubic spectral phase. The average temporal pulse profile has the standard ringing associated with cubic spectral phase—either before or after the main pulse, depending on the sign of the cubic spectral phase. When large amounts of linear chirp are used in the model, the temporal pulse broadens significantly (Fig. 7(c)), and the pulse spectrum becomes asymmetric in shape (Fig. 7(f)). Because of the interaction of the saturable absorber with the noise pulse, the leading edge of the temporal pulse is steep, and frequencies at the leading edge of the pulse are lost. Adding cubic spectral chirp to the highly linearly chirped pulse changes the leading edge of the temporal pulse, reducing its steepness at the top while little changing the average pulse spectrum.

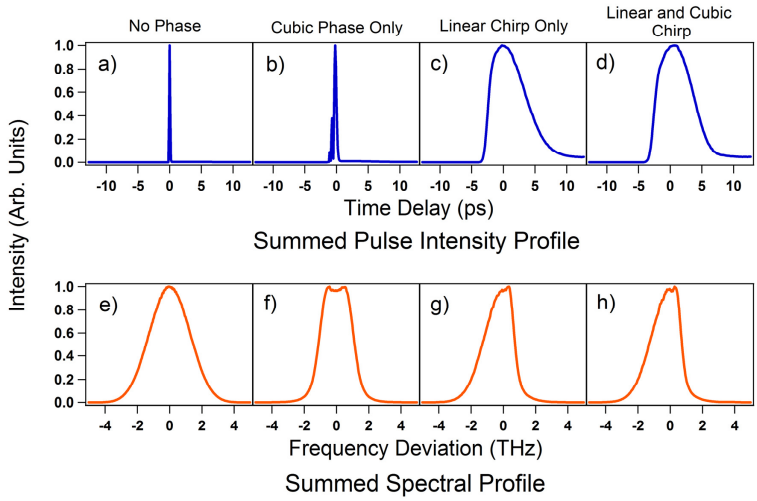

Fig. 7. Average pulses from the partial coherence model. The temporal pulses would be measured using a digital sampling oscilloscope (assuming adequate bandwidth) and the average spectra would be measured using an optical spectrum analyzer. Individual pulses within the pulse train vary randomly. Spectral and temporal shaping occurs only because the spectral chirp added together with the action of the saturable absorber.

Our partial coherence model does not take into account intensity interaction with the linewidth enhancement factor, which adds temporal phase proportional to the pulse intensity, nor does it take into account inter-pulse dynamics. This model also does not take into account multiple passes, only a single pass built up from noise. Although the photon lifetime is short, less than one round trip, large gain cross sections can still couple photons from one pulse to the next. However, the model does show that information about QDMLL operation, even when unstable, can be obtained from FROG measurements without algorithm convergence.

6. Conclusions

In summary, ultrashort optical pulses from a passively mode-locked quantum dot laser have been characterized using a highly sensitive FROG system. We have shown circumstances where widely-used measurement techniques result in misleading conclusions regarding semiconductor mode-locking and physics especially when mode-locking is unstable. For example, while autocorrelation measurements of mode-locked diode lasers provide necessary measurements for mode-locking, these measurements are not sufficient—autocorrelation alone cannot differentiate between stable and unstable mode-locking. Even digital sampling

#177027 - $15.00 USD Received 28 Sep 2012; revised 24 Nov 2012; accepted 12 Mar 2013; published 26 Mar 2013

oscilloscope measurements may also lead to misleading conclusions about individual pulse and stable device mode-locking. Under assumptions of the partial coherence model only full, simultaneous time-frequency pulse characterization methods, such as FROG, provide pulse measurements that are necessary and sufficient to prove mode-locking. To this end, we have demonstrated a collinear SHG FROG system using A-PPLN for full pulse characterization of QD MLLs. Our FROG system showed a much narrower mode-locking range of QDMLLs than autocorrelation, which allows the mode-locking range to be set arbitrarily. In addition, we have shown that mode-locking operational information can be determined from FROG measurements even when mode-locking is unstable, and we demonstrated that unstable mode-locking can be differentiated from stable mode-locking by simply examining the FROG spectrogram without the need for FROG retrievals. Furthermore, we showed that in many cases, QDMLLs that appear mode-locked from RF and autocorrelation measurements, but are not mode-locked from FROG measurements, can be described by a semi-empirical, partial coherence model.

Acknowledgments

This research was supported by the Air Force Research Laboratory under grant FA8650-07-M-1182, AFOSR under grants FA9550-12-1-0049 and FA9550-10-1-0276, and this material is based upon work supported by the National Science Foundation under Grant No. 0930697.

#177027 - $15.00 USD Received 28 Sep 2012; revised 24 Nov 2012; accepted 12 Mar 2013; published 26 Mar 2013